Structural Modeling of the Area East the Gulf of Suez and Sinai from Interpreted Gravity and Magnetic Anomalies

Mebed M.[1], Hassan. S. S.[2], M. Bekhet[2]; and Ali. F. Hammam[1]

[1]Egyptian Mineral Resources Authority (EMRA), Cairo, Egypt.
[2]Geology Department, Faculty of Science**,** Al-Azhar University, Cairo, Egypt.
Geo_alifathy@yahoo.com

Abstract: This work deals with the evaluation of the structural modeling of the east Gulf of Suez and Sinai from magnetic and gravity data. The main target of the present study is to establish basement configuration and basement related structural elements if a number of positive structural features will be identified from the results of the geopotential data interpretation. Future hydrocarbon exploration may be encouraged in the study area. The basement related faults/lineament maps were generated through the processing and interpretation of the gravity and magnetic data. These results were further refined the studies of 2- D modeling. The study illustrated that, the igneous basement rocks are the main causative bodies for the magnetic anomalies in the study area. Two main average interfaces at depths of 2.4 km and 10 km, respectively blow the measuring level, were revealed through the application of local power spectrum on the total magnetic map. The depth to the basement variation from east to west and the basement depths ranging approximately from 800 m to more than 7 km below sea level. A number of positive structural features were identified which may provide lead for future hydrocarbon exploration. The depths to the basement map indicate the sediment thickness exceeds 7 km at some places. The general trends of basins and sub basins; those found in the southern, northern and other places of the study area with mainly NE-SW direction, whether the deepest places is located in northeastern, northwestern and central parts on map with NE-SW, NW-SE and E-W directions. The processing and interpretation of potential field data yielded basement faults and structural framework of the area. The general basement faults trends are striking mostly in NE-SW and NW-SE directions.
[Mebed M., Hassan. S. S., M. Bekhet; and Ali. F. Hammam . **Structural Modeling of the Area East the Gulf of Suez and Sinai from Interpreted Gravity and Magnetic Anomalies.** *Nat Sci* 2017;15(10):44-56]. ISSN 1545-0740 (print); ISSN 2375-7167 (online). http://www.sciencepub.net/nature. 7 doi:10.7537/marsnsj151017.07.

Key word: Structural modeling, Lineament, Magnetic data, Gravity data, Basement depth, Sedimentary thickness.

1. Introduction

The study area is located in east Gulf of Suez, It covers an area of about 2710 km^2, between latitude 28° 15′ 00″ N and 28° 45′ 00″ N and longitude 33° 15′ 00″ E and 33° 45′ 00″ E (Fig. 1). The main objective of this study is to establish basement configuration and basement related structural elements, if a number of positive structural features will be identified from the results of the geopotential data interpretation; that can be promising location for hydrocarbon exploration in the future.

The gravity data of study area is obtained from the Bouguer gravity map executed by The Egyptian Geological Survey and Mining Authority (EGSMA, 2003) with scale 1:500,000and contour interval of 1 mGal.

The magnetic data obtained from the total magnetic intensity map executed by The Egyptian Geological Survey and Mining Authority (EGSMA, 2003) with scale 1:500,000.

The gravity and magnetic data were subjected to different processing techniques using Oasis montaj software version 8.3.3 (Geosoft, 2014).

2. Geologic setting

The geology of the study area ranges from Precambrian basement rocks to the Quaternary deposits. According to the Egyptian Geological Survey map (EGSMA, 2003), the Quaternary deposits cover the basement rocks along the Gulf of Suez and Gulf of Aqaba.

The basement rocks (Precambrian) occupy the southern part of the studied area (Fig.2), along the Gulf of Suez and Gulf of Aqaba. On the other hand, the Palaeozoic rocks are present in the middle part while the Mesozoic rocks covered the eastern and western parts of the area.

The Red Sea and Gulf of Suez basins consist of a high faulted block more than 100 000 km2 in size that contains block-faulted trapping configurations in the Gulf of Suez. This unit includes coastal areas of the Red Sea and the Southern Gulf of Suez.

3. Structural setting

The study area is characterized by tilted fault blocks which represent a segment of the very long chain of connected fault blocks extending from NW to SE and including Hammam Feraun, Nazzazat, Ekma, Durba and Araba blocks. This chain of fault blocks represents most of the NE-dip province of Moustafa (1973) or the central half – graben of Moustafa

(1993). The northeastern part of the study area occupied by Al Tih and Egma plateau (Fig.2), they are dipping generally to the north. The Tectonic setting of the study area is in relation to the Suez rift.

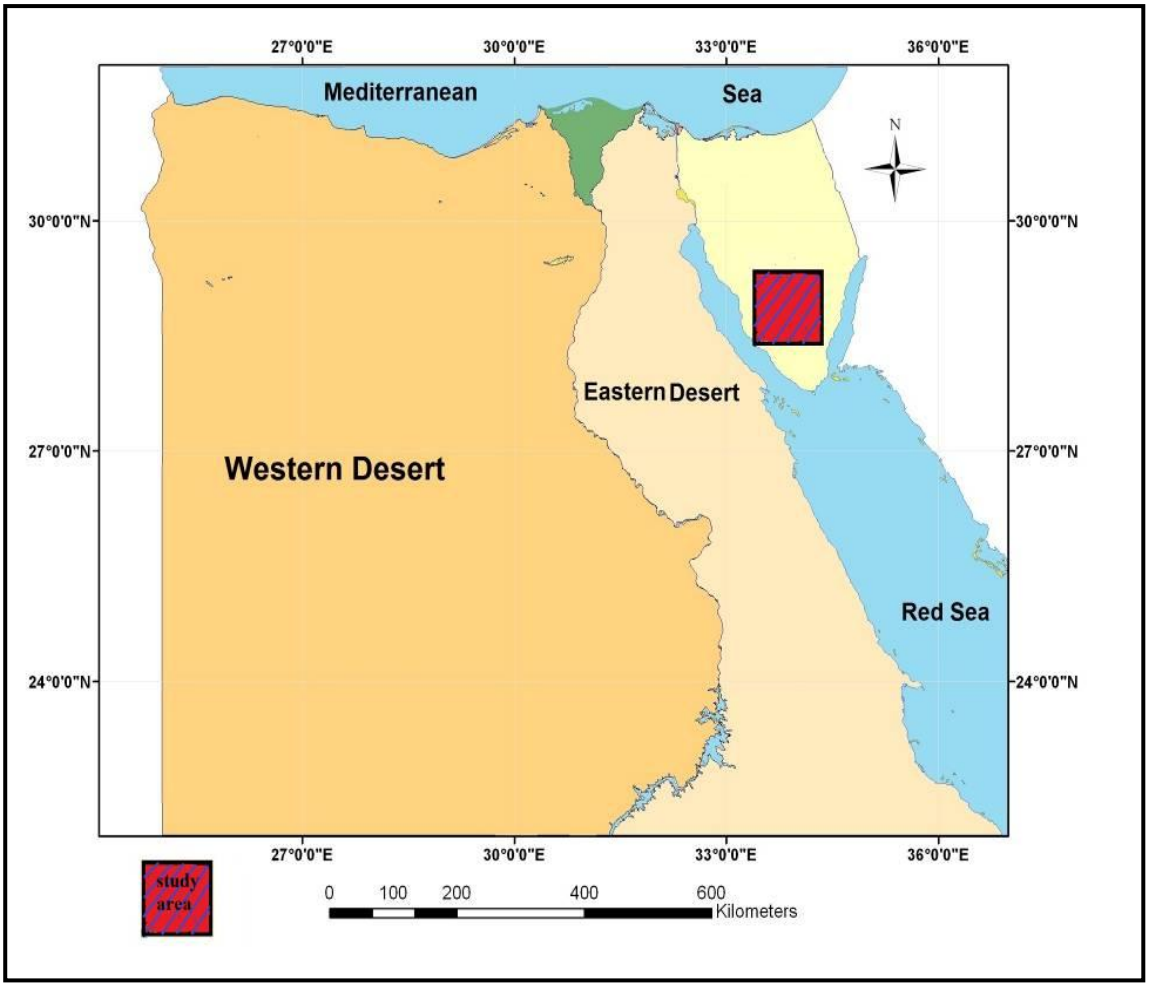

Fig. (1): Map of Egypt showing the location of the study area

4. Processing of Geophysical data

4.1. Gravity method

Because an object on the earth's surface is attracted by the mass of the earth, the gravity exploration method detects variations in the densities of the subsurface materials by measuring gravity at the surface and analyzing the differences in the recorded values (Burger, 1992).

Different rock densities produce small changes in the gravity field and can be measured using portable instruments known as gravimeters (Milson, 1989). The end product of a gravity field survey (after applying the necessary corrections) is usually a contoured anomaly map, the so-called Bouguer gravity anomaly map. The aim of geophysicists is to determine the various characters from the study of the shape, amplitude, sharpness and frequency of the anomalies.

Therefore, a lot of techniques were developed to enhance the gravity map for the interpretation purpose. Some of these techniques are well – suited in a computer package named as MAGMAP, which produced by Oasis Montaj software version 8.3.3, (Geosoft programs, 2014).

4.1.1. Description of Gravity data

The gravity data presented in this study are collected by the Egyptian Geological Survey and Mining Authority (EGSMA, 2003). Gravimetric field measurements are carried out with the CG-3 Autograv (automated Gravity meter) made by Scintrex.

The ENVI–MAG (Scintrex, Canada) magnetometer with accuracy of 0.01 gammas was used to measure the total magnetic field in the filed measurements.

After the recording of gravity and magnetic data, several corrections are applied to the data to produce grid versions of Bouguer gravity. However in many

cases it is possible to apply various filtering and transformation processes prior to the display of the data sets to produce secondary products with obviously improved information content.

4.1.2. Enhancement of the gravity data

The inspection of the Bouguer gravity anomaly map (Fig.3) reveals that gravity maximum values in the south and northwestern part of the area and reach to about 9.1 mGal and decrease to reach its minimum value in the northeastern part of the area (-55.50 mGal). The area under consideration can be subdivided into two highest magnetic portions and one lowest magnetic portion.

Two highest magnetic portions occupies in the south and northwestern parts of the area and extend from southeastern corner of the map to eastern central part with high and moderate gravity anomalies and take NE-SW direction. The one lowest magnetic portion nearly at the extreme northeastern part of the area with low gravity anomalies and takes NW-SE direction.

The south and northwestern parts of high gravity anomalies are separated from the extreme northeastern low anomalies by high gradient elongated contour that may be associated with major fault and take NE-SW direction.

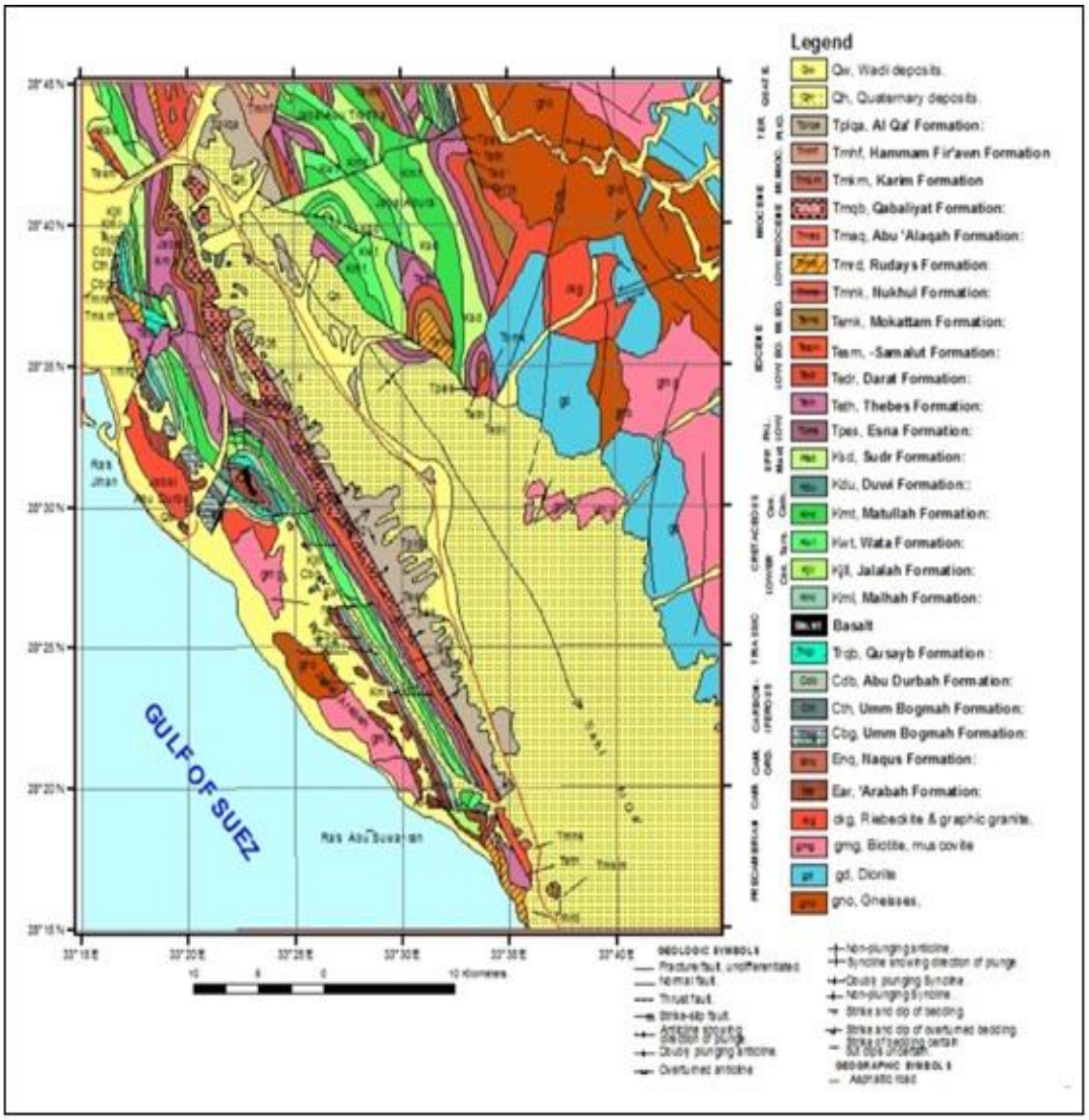

Fig. (2): Geological map of the study area (after EGSMA, 2003)

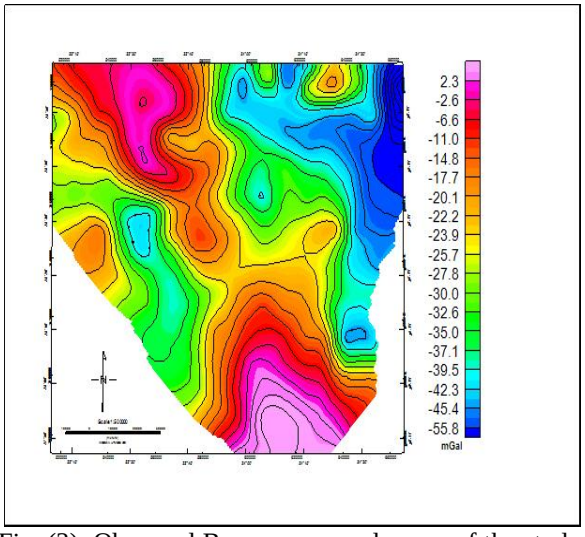

Fig. (3): Observed Bouguer anomaly map of the study area

4.1.3. Radially averaged power spectrum

The Radially averaged power spectrum illustrated that (Fig.4) deep sources are pronounced by wavenumbers from 0.044 to 0.084 cycles / k-unit, while the shallow sources by wavenumbers between 0.084 and 0.24 cycles / k- unit for first level of residual and between 0. 24 and 1.24 cycles / k- unit for second level of residual. The noisy part of the spectrum is more than 1.24 cycles / k- unit.

The estimated average depths to the regional and residual sources are 7.9 km and 0.9 km.

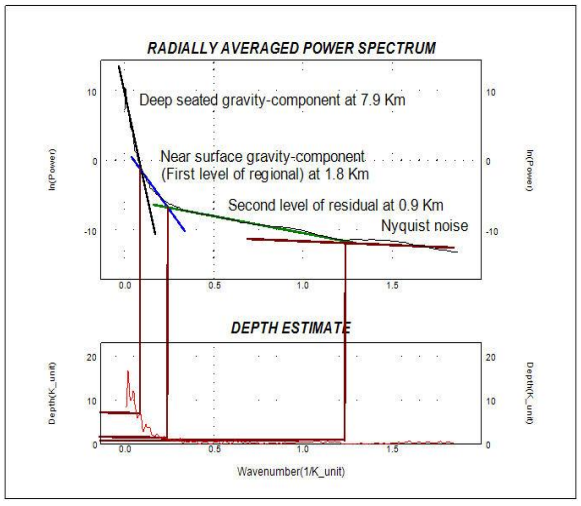

Fig. (4): Radially averaged power spectrum and depth estimate of gravity data

4.1.4. Regional-residual separation

The Bouguer gravity anomaly map is separated directly into regional and residual components (Figs.5 and 6).

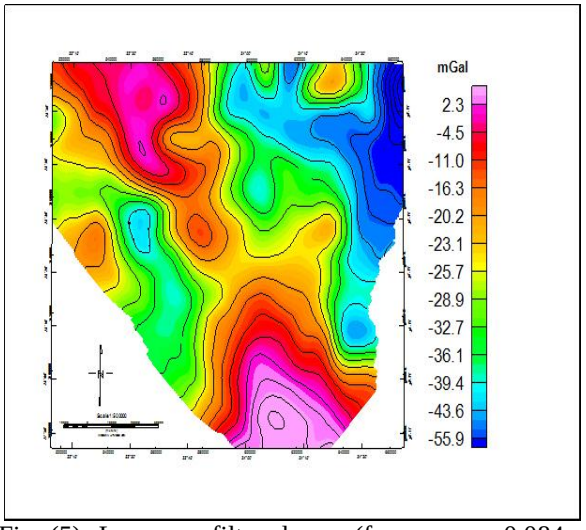

Fig. (5): Low-pass filtered map (frequency = 0.084 - 0.24 cycles/k- unit)

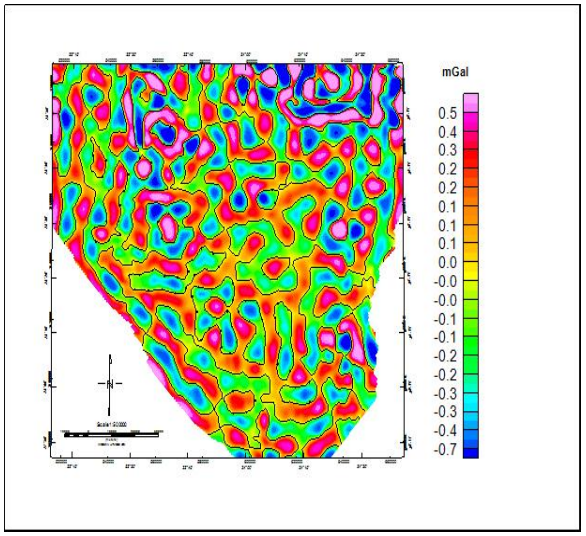

Fig. (6): Band-pass filtered map (frequency = 0.24 - 1.24 cycles/k- unit)

The low-pass (regional) gravity map: reveals that (Fig.5), the principle NW-SE gradient is still occupying nearly central part of the area and extends from southern part of the area to northwestern corner of the map (Fig.5). While, the NW-SE gradient disappeared and major fault is still founding and take trend NW-SE.

The band-pass for the higher frequency (residual) gravity map: (Fig.6) represents actually the distribution of the gravity field at a shallow depth and after removing the regional effect. Thus, the map reveals considerable frequencies of high and low gravity anomalies and of limited aerial extension, different amplitudes and varying trends. These parameters reflect the difference in anomalies, sources, depths, compositions and structure setting.

Therefore, these local anomalies can be differentiated into three groups; one of them is trending NW-SE and locating the southeastern and western parts with medium gravity anomaly (Fig.6). The second group is trending NE-SW and locating the northeastern to southwestern parts of the area with high and medium gravity anomaly. The third group is circular anomalies and representing in the northern and central part of the area (Fig.6).

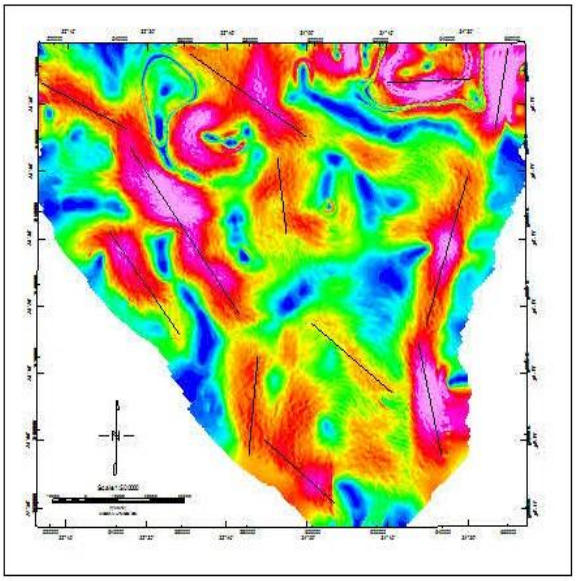

Fig. (7): Horizontal gradient of the gravity data of the study area

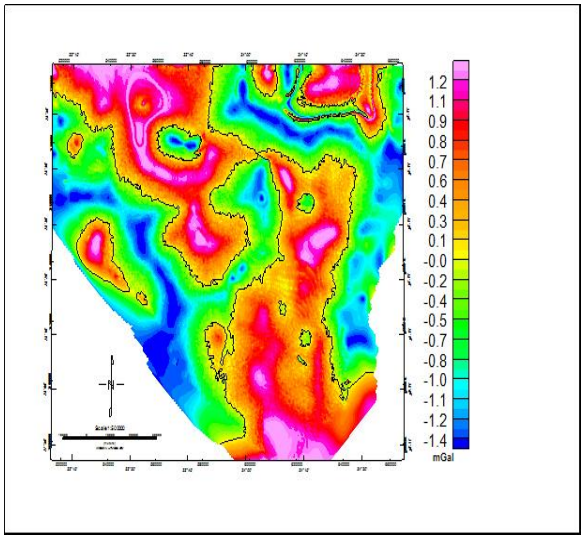

Fig. (8): Tilt derivative map of gravity data of the study area (at contour interval 0)

4.1.5. Horizontal Gradient (HG)

The horizontal gradient method has been used intensively to locate boundaries of density and susceptibility contrasts from gravity and magnetic data. The horizontal gradient of the gravity or magnetic anomaly caused by a tabular body tends to overlie the edges of the body if the edges are vertical and well separated from each other (Cordell, 1979 and Cordell and Grauch, 1985).

The greatest advantage of the horizontal gradient method is that it is least susceptible to noise in the data, because it only requires the calculations of the two first-order horizontal derivatives of the field (Phillips, 1998).

Generally, the horizontal gradient map (Fig.7) locates the boundaries and edges of the body by horizontal gradient method where appear the high anomalies (red color) in the map represented the contact and boundaries place.

4.1.6. Tilt Derivative (TDR)

Tilt derivative (TDR) of gravity and/or magnetic anomaly fields is a method for edge detection (Miller and Singh, 1994, Verduzco et al., 2004 and Oruc and Kenskinsezer, 2008).

The Tilt derivative map shows (Fig.8) edges of contact and clear boundaries between structure units in the central, northern and southern parts.

4.2. Magnetic method

The magnetic method, as used in geological exploration, is possibly the method versatile of the methods of geophysics, as it can be applied to both deep and shallow structures, and relative to other methods, measurements can be relatively cheaply obtained for both local and regional studies (Burger, 1992).

Magnetic method is based on the measurements of small variations in the magnetic field, which may be caused by heterogeneities in the composition of the basement rocks or by structural or topographic relief of the basement surface. These variations may be measured at the surface or more commonly by suitable instruments carried in an air craft and interpreted to determine the depths to the basement rocks and, thus, defining the thickness of the sedimentary cover (Nettleton, 1976).

4.2.1. Total magnetic data enhancement

The total intensity magnetic map (Fig.9) can be divided into three zones according to magnetic characters:

1-The highest magnetic anomalies area is in southern and northern part of the area and have NE-SW trend.

2- The moderate magnetic anomalies are in western part of the area and has NW-SE trend.

3-The lowest magnetic anomalies is in northeastern and central part of the area and has NE-SW trend.

On the other hand, the clear investigation of the total intensity magnetic map of the study area (Fig.9) revealed that the magnetic field increase up in the area

with maximum relief of about 42636.467 nT in southern and northern part of the area and decrease to minimum of about 42155.046 nT in the northeastern part of the area. The general magnetic trends of the area are almost NE-SW and NW-SE. The highest magnetic anomalies at southern and western part is separated from lowest magnetic anomalies in the northeastern part of the area by steep gradient indicate that it is structurally controlled by a major fault trending in NW-SE direction.

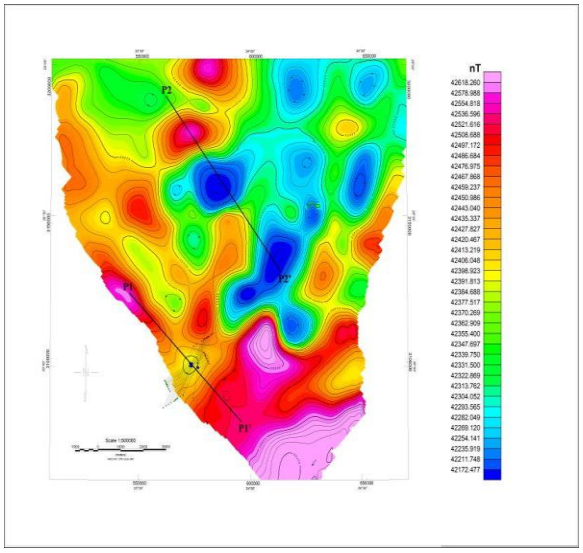

Fig. (9): Total intensity magnetic map of the study area

4.2.2. Reduction to the northern magnetic pole (RTP) map

The method of reduction to the pole (RTP) is used to remove effect both positive and negative responses. So that the data appear as if observed at the pole, where the magnetic field is vertical (Kearey et al., 1994).

The total intensity magnetic map was reduced to the northern magnetic pole by using 2-D wave number filtration utilizing the known inclination and declination of the study area (the total magnetic intensity is 42730.76 gammas, inclination and declination angle are 42.24 degree and 3.1 degree, respectively). These parameters are used to yield the reduced to north magnetic pole and construction of the RTP magnetic map (Fig.10).

The clear investigation of the total intensity magnetic map reduced to the pole in the study area (Fig.10) revealed that the magnetic field increases up in the area with maximum relief of about 42363.467 nT in eastern and south eastern part of the area and decrease to minimum of about 42155.046 nT in southwestern part of the area of the area. The general magnetic trends of the area are almost NW-SE and NE-SW.

The area under consideration could be zoned magnetically into two different zones having various magnetic characters. The first one is represented by almost high positive and long wavelength anomalies and is situated in southern and northeastern parts of the area and has ENE-WSW and NW-SE trends. The second magnetic zone is represented by low and medium magnetic anomalies and is situated in northern and southwestern parts of the area and have NE-SW trend.

The high magnetic zone in southern and northeastern parts is separated from medium magnetic zone in central part of the area by steep gradient indicate that it is structurally controlled by fault having major axis NE-SW and The high magnetic zone in northwestern part is separated from low magnetic zone in northern part of the area by steep gradient indicate that it is structurally controlled by fault having major axis NE-SW.

4.2.4. Regional-residual separation

Regional and residual maps were used to determine the shallow and deep structural features affecting the study area that could help to give a satisfactory picture of the basement configuration and to determine the tectonics of the study area.

The low-pass (regional) magnetic map: This map (Fig.12) shows that high magnetic anomaly still occupies southern and western parts of the area and the anomaly is closed with NNW-SSE direction and low magnetic anomaly still occupies the northeastern part. Whereas high magnetic anomaly in southern and western parts of the area is locate beside low magnetic anomaly in the northeastern part this may indicate a proposed fault with NW-SE and NNE-SSW directions.

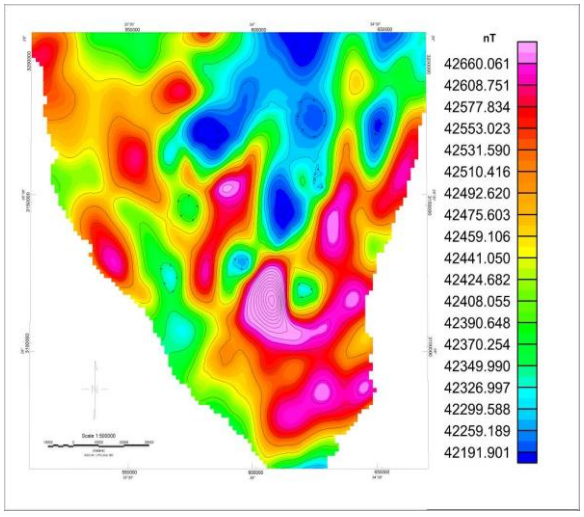

Fig. (10): Reduced -To - pole magnetic map of total intensity magnetic data of the study area

4.2.3. Radially averaged power spectrum

As a result of visual inspection of the two-dimensional power spectrum curve (Fig.11).

The estimated average depths to the regional and residual sources are 2.4 km and 10 km.

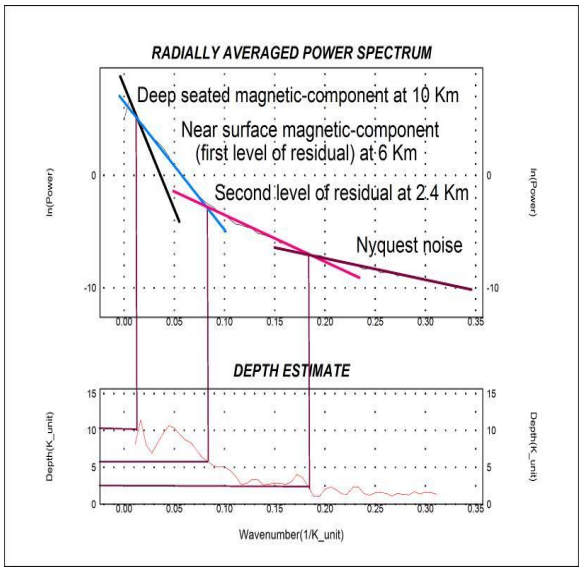

Fig. (11): Radially averaged power spectrum and depth estimate of magnetic data

The band-pass (residual) magnetic map: Visual inspection of this map (Fig.13) shows several alternative negative and positive magnetic anomaly zones, which possess a general NE-SW direction. These zones are dissected by many faults in different directions. It shows that there is zone in the southern and central parts has high (positive) magnetic anomaly, take NE-SW direction. The northwestern part has low (negative) anomaly.

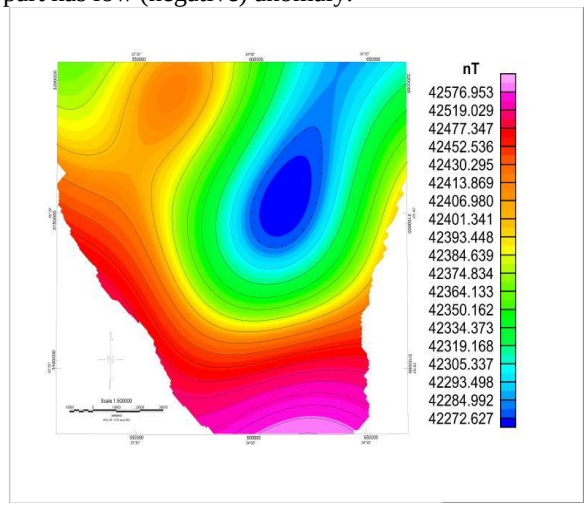

Fig. (12): Low-pass filtered map (frequency = 0.002 - 0.01 cycles / k-unit)

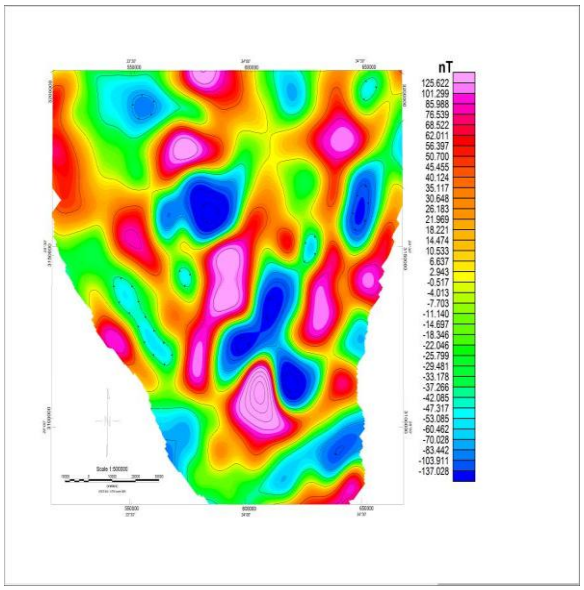

Fig. (13): Band-pass filtered map (frequency = 0.01 - 0.08 cycles / k- unit)

4.2.5. Vertical derivative

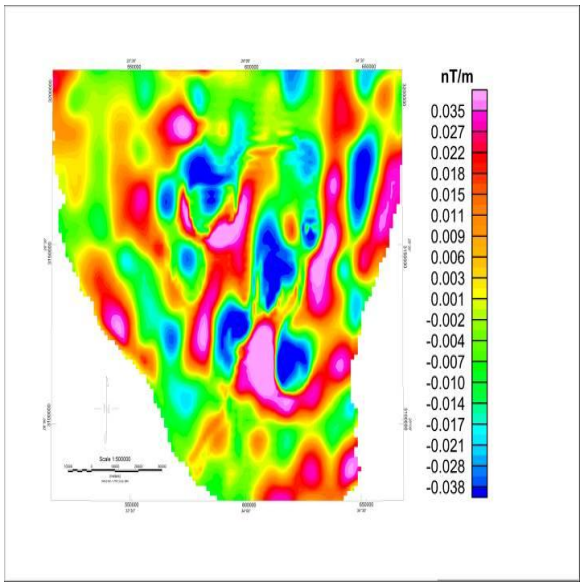

Fig. (14): First vertical derivative of the study area

First vertical derivative field map is often used to detect edges and geologic boundaries in data (Henderson and Zietz, 1949). The vertical derivative is commonly applied to RTP magnetic data to enhance the shallow geologic source in the data.

Vertical derivative maps, usually the first or second vertical derivative, accentuate gradients along edges of shallow magnetic sources. Hence, they are used to locate edges of magnetic bodies and to

emphasize sources at shallow depths (Dobrin and Savit, 1990).

The main feature the first vertical derivative map (Fig.14) are clearly identified and local anomalies become more prominent than of total magnetic intensity map. There are edges and geologic boundaries in southern and eastern parts with trends N-S, NE-SW, NW-SE, also in the western part with NW-SE and E-W and in the central part with NE-SW direction.

4.2.6. Horizontal gradient (HG)

The horizontal gradient map (Fig.15) shows boundaries and edge between the rock units.

Inspection of this map show high anomalies in some places, where represents location of boundaries and edges like that present in north, south,, eastern, central parts and other places in the map.

4.2.7. Tilt Derivative (TDR)

The tilt derivative of the RTP magnetic data of the study area was calculated (Fig.16). The zero contour of tilt derivative may be used to trace susceptibility contacts.

The dominant fault trends in the area of study are NE-SW and NW-SE. This map is similar to the first vertical derivative map (Fig.14).

5. Interpretation of Geophysical data

5.1. Magnetic data interpretation

The depth to basement extension to Oasis montaj provides an automated method for determining the position (i.e., distance along the profile and depth), dip (i.e., orientation) and intensity (e.g., susceptibility) of magnetic source bodies for a magnetic profile. The extension includes three different depths to basement techniques: Werner Deconvolution, Analytic Signal and Euler Deconvolution.

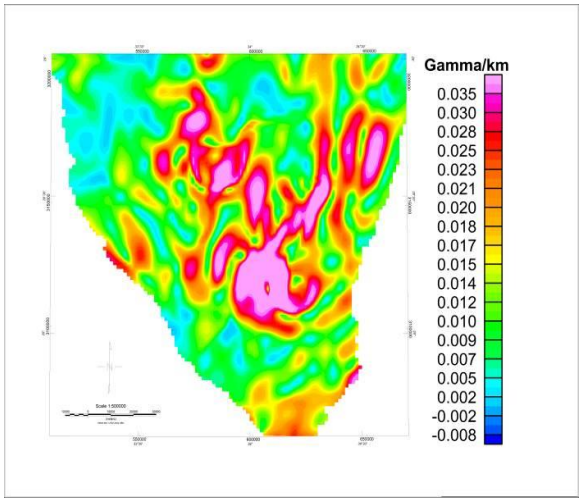

Fig. (15): Horizontal gradient of RTP magnetic data of the area

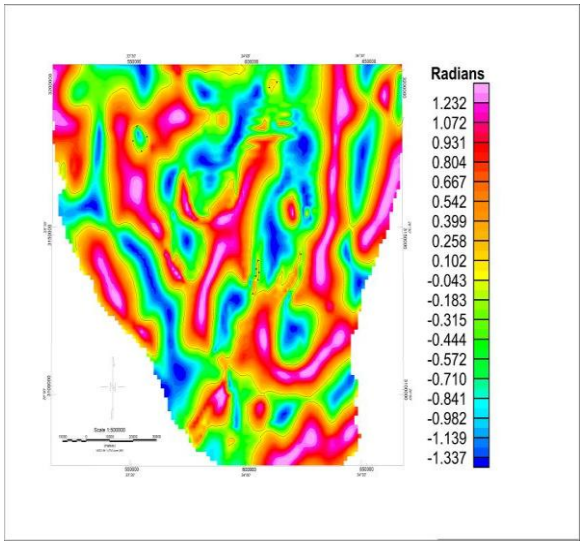

Fig. (16): Tilt derivative map of RTP magnetic data of the study area (at contour interval zero)

5.1.1. Euler Deconvolution

Euler Deconvolution technique is carried out by using Oasis montaj Ver, 8.3.3 with structural indices (SI) = 1 according to Reid, et.al (1990). The solution of the magnetic anomaly maps with SI=0 for probable contact and SI=0.5 for fault at depths are represented in (Fig.17) for the study area.

Also, Depth estimation by 3D Euler Deconvolution technique was used for rapid estimation of geologic contacts at different levels in the area under consideration. The total magnetic and contacts solution depths map (Fig.17) reveals the subsurface contacts depths range from 0 to more than 7 km with trending N-S, NE-SW, NW-SE and E-W.

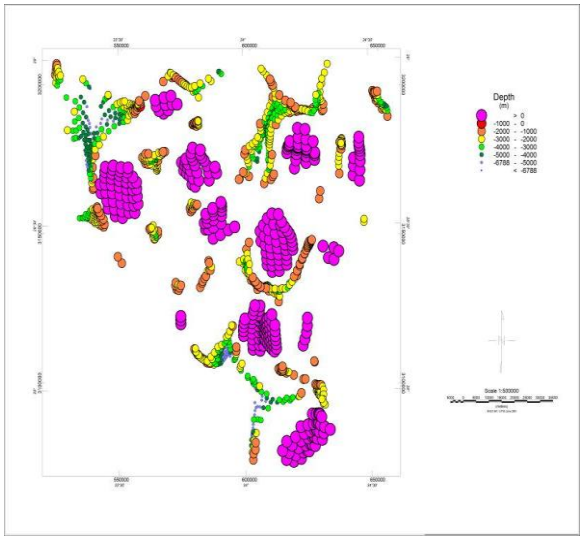

Fig. (17): Total intensity magnetic and contacts solution depths map

5.1.2. Source Edge Detect (SED)

The Source Edge Detection (SED) function locates edges (i.e. geological contacts) or peaks from potential field data by analyzing the local gradients. The SED function estimates the location of abrupt lateral changes in magnetization or mass density of upper crustal rocks. Its procedure is to identify maxima on a grid of horizontal gradient magnitudes.

Using the technique of a database of source edge locations are derived from a grid of total magnetic field or gravity (Phillips, 2000 and Blakely, 1986). A map is produced with symbols representing locations and gradient directions of potential field anomalies. You can distinguish between gradients that are in 1, 2, 3, or 4 directions.

The edges and geologic boundaries were represented by source edge detect technique in (Fig.18) and the rose diagram in (Fig.19) show the trend take NWW-SEE and NEE-SWW direction as main trend and E-W and N-S trend.

5.1.3. Analytical Signal

Analytic signal is an automated function that enables us to determine depth solutions from gravity and magnetic maps or profiles Roset et al. (1992) and Macleod, (1993).

Figure 9 Shows 2 profiles on total intensity magnetic map which used for analytical signal.

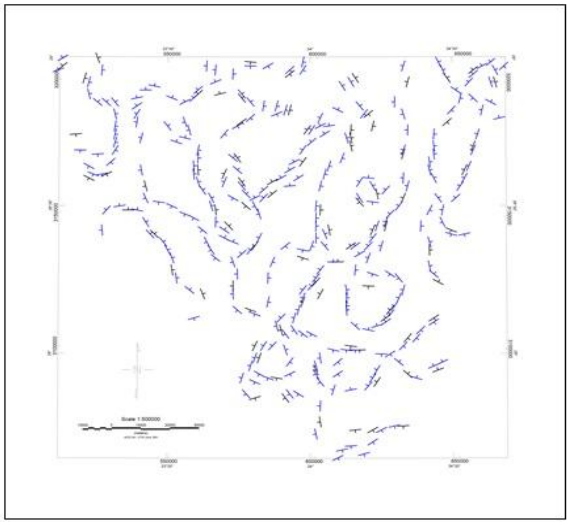

Fig. (18): Source Edge Detect map in 4 direction of the study area

Profile P1-P1': Figure 20 shows depths of z-dikes and z-contacts along profile. Depths of dikes range between 3860 m as maximum and 793.8 m as minimum with mean depth 1841 m. Whether contacts is reach to 3985 m as maximum and 102 m as minimum with average depth 1675.9m.

Profile P2-P2': Figure 21 shows depths of z-dikes and z-contacts along profile. Depths of dikes range between 3999 m as maximum and 1044 m as minimum with mean depth 2728 m. Whether contacts is reach to 3997 m as maximum and 96.7 m as minimum with mean depth 1998.7 m.

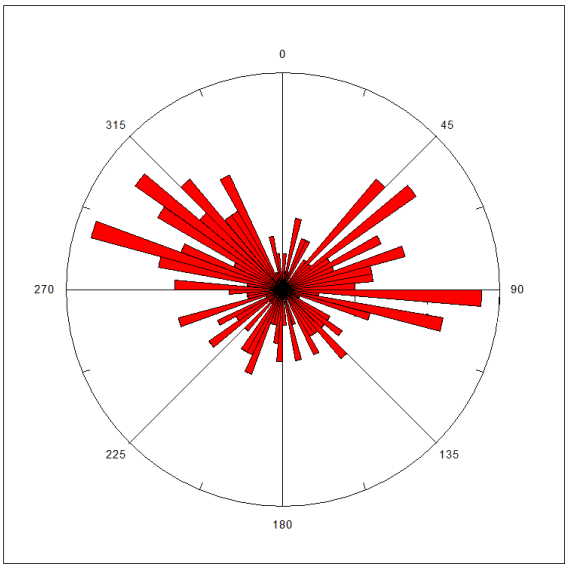

Fig. (19): Rose diagram result from Source Edge Detect map of the study area

5.1.3. Werner Deconvolution (solutions)

The Werner Deconvolution technique as introduced by Werner (1953) has been applied to obtain the basement depth and this technique has been applied to obtain the basement depth.

Profile P1-P1': Figure 22 shows depths of z-dikes and z-contacts along profile. Depths of dikes range between 3958 m as maximum and 34 m as minimum with mean depth 693 m. Whether contacts is reach to 2023 m as maximum and 4.7 m as minimum with average depth 509 m.

Profile P2-P2': Figure 23 shows depths of z-dikes and z-contacts along profile. Depths of dikes range between 3997 m as maximum and 4.8 m as minimum with mean depth 1405 m. Whether contacts is reach to 3939 m as maximum and 17 m as minimum with average depth 981 m.

5.2. Gravity data interpretation

5.2.1. Euler Deconvolution

Faulting and contacts pictures at different levels of the gravity data for the study areas are carried out using Euler Deconvolution technique using Oasis montaj Ver. 8.3.3, with different structural indices (SI) according to Reid, et al (1990).

In the present study, Euler Deconvolution technique was used to determine the depth, location and trend of the faults in the area under investigation.

Depth estimation by 3D Euler Deconvolution technique reveals the subsurface shallow and deep contacts depths range between 0 km to 5 km. These

structural may be useful in defining the location of faults or fractures in overlying rocks, which may be acted as pathways for mineralizing solutions, groundwater or petroleum.

6. Two Dimensional (2-D) forward modeling

2-D forward modeling has been performed on two preselected profiles (Fig.4-4), one of them through five wells, Sinai-1, Sinai-5, Sinai-6, Sinai-7 and Garra Marine-4 borehole also through 33 seismic lines, using GM-SYS modeling version.4.9 (Geosoft,2014) which was established by North Geophysical Association

Profile P1-P1': has been taken along NW-SE direction with length 116 km (Fig.25) and shows variation in the basement surface and passing through five wells (Sinai-5, Sinai-1, Sinai-7, Garra Marine-4 and Sinai-6 borehole) this wells is located at 30 km, 42 km, 58 km, 71 km and 103 km respectively along the profile.

The gravity and magnetic modeling of this profile indicates that the first part of the profile exhibits deeper values for the basement surface of about 3388 m and locate in SW direction and the depth of the basement surface become more shallower about 1888 m with NE direction at 75 km from starting point (NW) from the profile.

The best place that may be used as basin at the beginning of the profile after 23 km there is a normal fault with suitable.

Profile P2-P2': has been taken along N-S direction with length 87 km (Fig.26).

The gravity and magnetic modeling of this profile indicates that the depth to the basement surface occurs at shallowest surface of 753 m in the far south direction, whereas the deepest basement surface reaches to about 4479 m after 15 km from the beginning of profile.

This profile has normal faults forming horst and graben, so this profile may represent a good basin to accumulate petroleum or water.

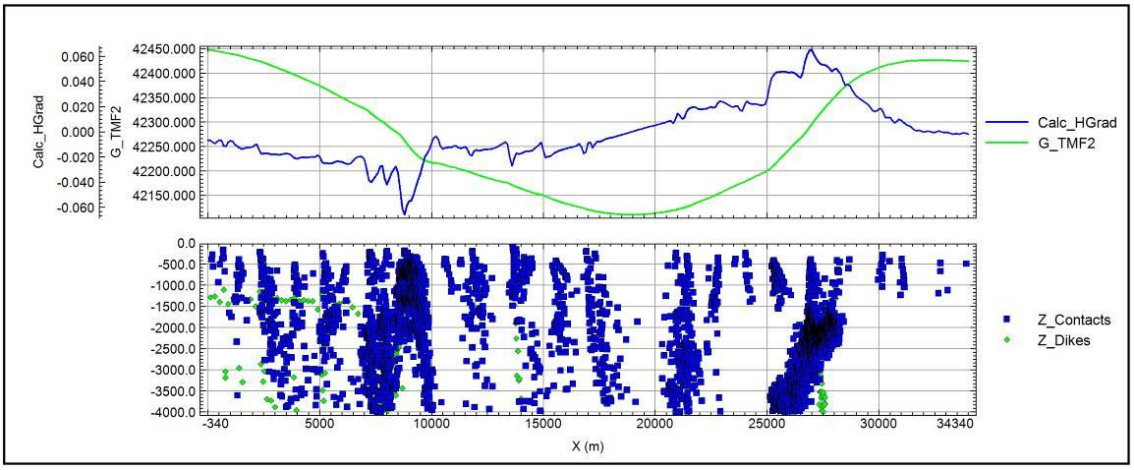

Fig. (20): Shows analytical signal with depths of z-dikes and z-contacts along profile P1-P1'

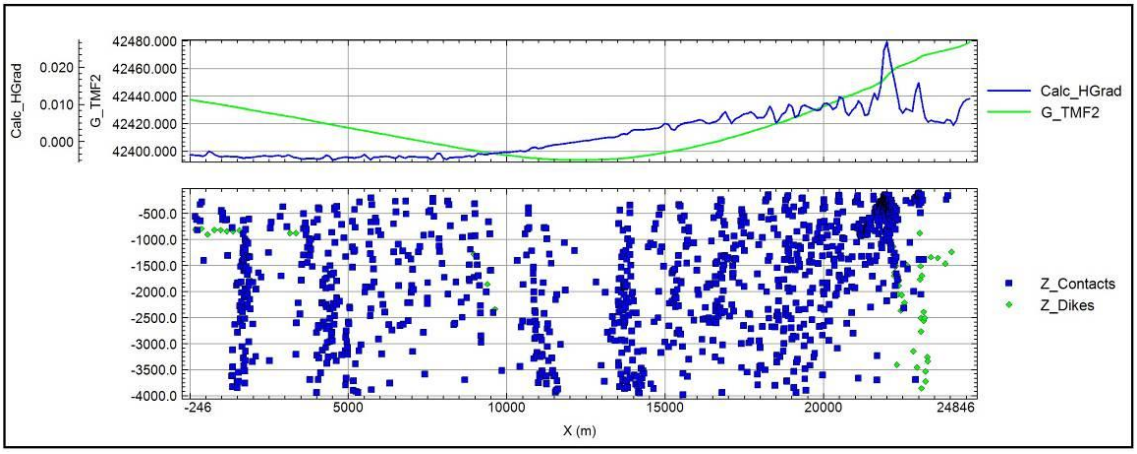

Fig. (21): Shows analytical signal with depths of z-dikes and z-contacts along profile P2-P2'

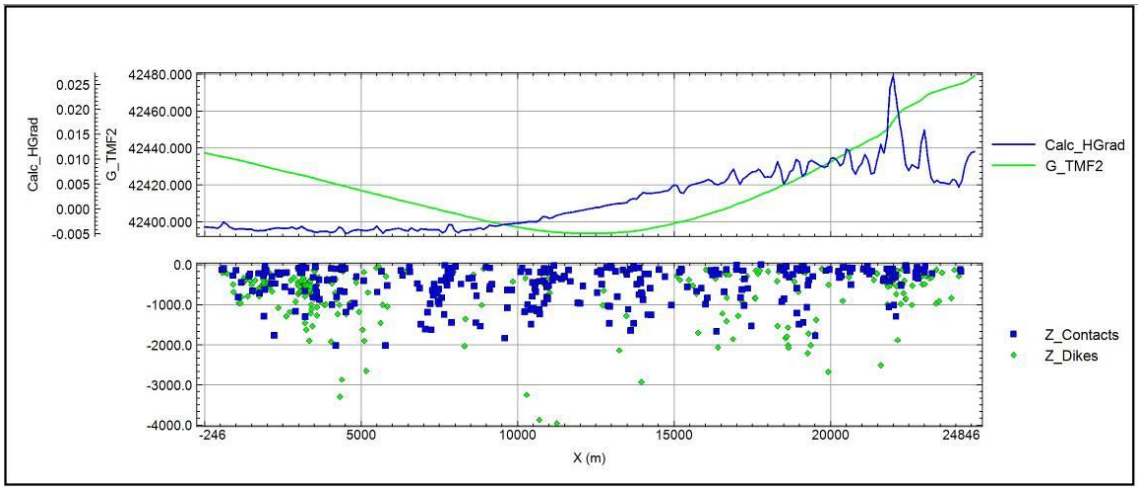

Fig. (22): Shows Werner solution with depths of z-dikes and z-contacts along profile P1-P1'

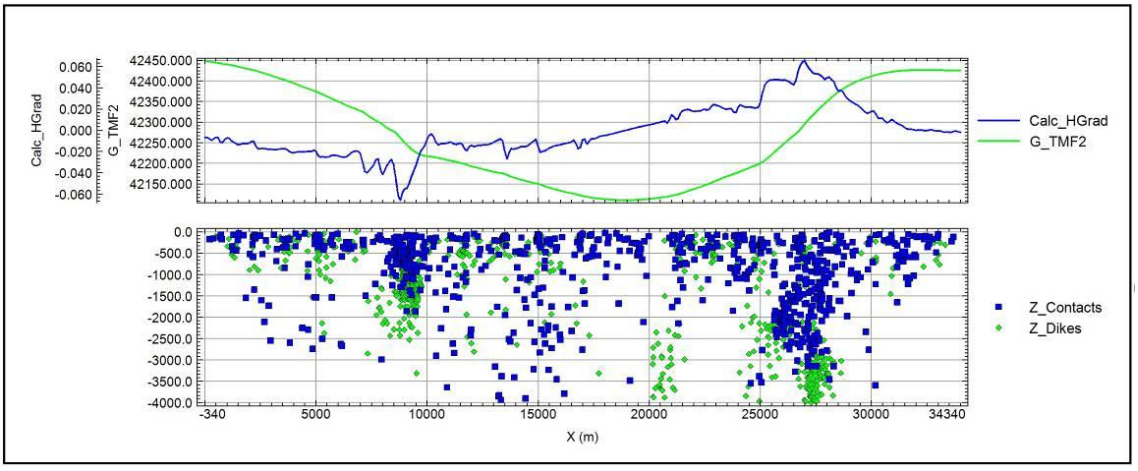

Fig. (23): Shows Werner solution with depths of z-dikes and z-contacts along profile P2-P2'

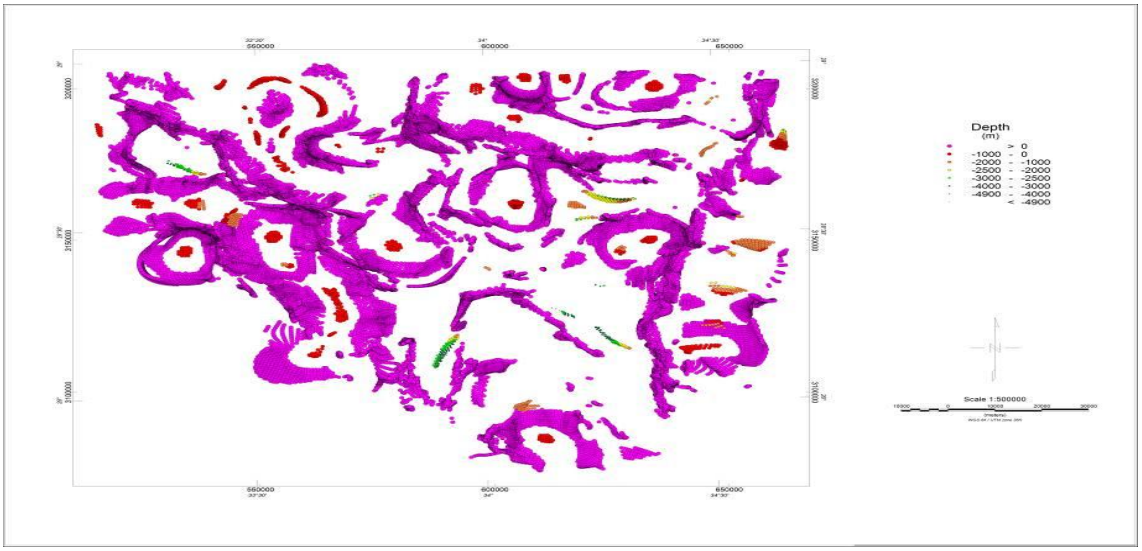

Fig. (24): Euler solution of the gravity data of the study area with SI=0

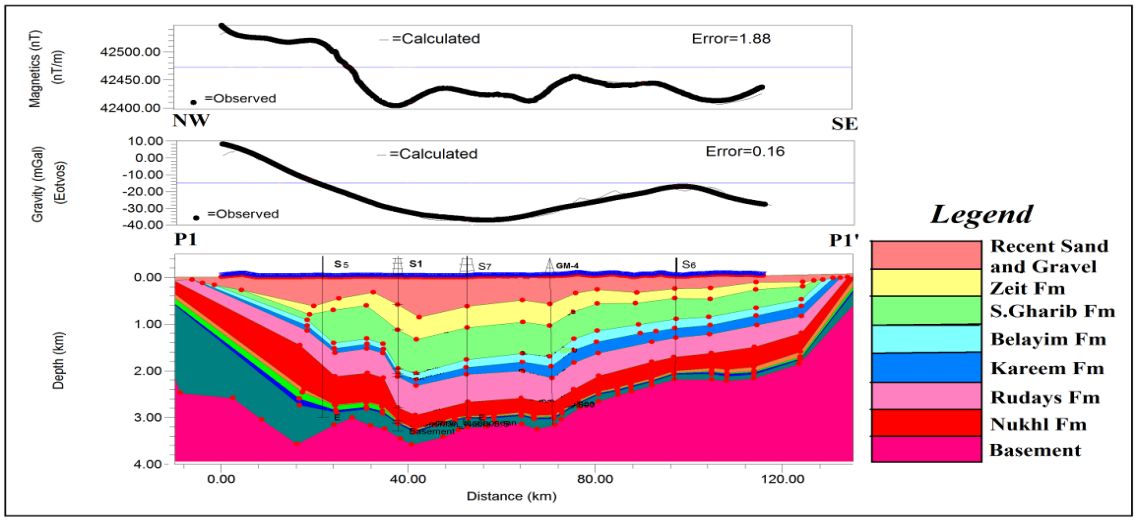

Fig. (25): 2-D modeling of the Gravity and magnetic of profile P1-P1'

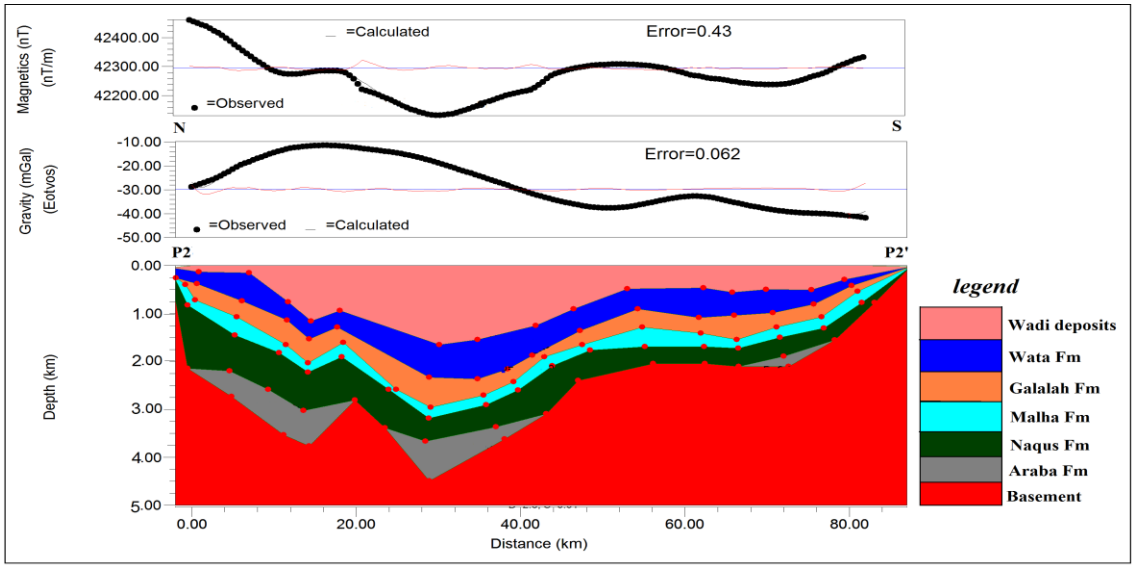

Fig. (26): 2-D modeling of the Gravity and magnetic of profile P2-P2'

Conclusion

This study was carried out using different geophysical tools (magnetic and gravity methods). The data were analysed using the most advanced and suitable techniques. The results of structure analysis indicate that most of the predominant directions are NE-SW and NW-SE directions that related to Gulf of Suez and Red Sea tectonics. The application of Euler deconvolution estimate the position of the subsurface intruded magnetic bodies indicates that the depth to these bodies ranges from 0 km to about 7 km. Furthermore, application of the analytical signal method confirms the result deduced by the Euler deconvolution technique. The technique prints out a complete view for the geometry of the basement surface where the depth ranges between 0 km to more than 5 km. The results indicate that the average depths of the causative magnetic bodies within the study area having average depths of 2.4 and 10 km below the measured level, for the near-surface, second level of residual and deep-seated magnetic effects respectively.

Also the results indicate that the structures of the area are related to Gulf of Suez, and Red Sea tectonics. These structures extend from the basement rocks upward into the sedimentary sequences and divide the area into several major faulted blocks that have great important in sealing the oil traps. This work is considered a guide line for further exploration process and geophysical works.

References

1. Blakely, R. J., and Simpson, R. W., (1986): Approximating edges of source bodies from

magnetic or gravity anomalies. Geophysics 51, 1494–1498.
2. Burger, H. R., (1992): Exploration geophysics of the shallow subsurface; Prentice and Hall, 489p.
3. Cordell, L., (1979): Gravimetric expression of graben faulting in Santa Fe country and the Espanola basin, New Mexico in Ingersoll, R.V., ED., Guidebook to Santa Fe country, New Mexico Geol. Soc. Guidebook, 30th field conference, 95-64.
4. Cordell, L., and Grauch, V. J. S., (1985): Mapping basement magnetization zones from aeromagnetic data in the San Juan basin, New Mexico. In Hinze. W. J., Ed. The utility of regional gravity and magnetic anomaly maps: Sot. Explor. Geophys. 181-197.
5. Dobrin, M. B., and Savit, C. H., (1990): Introduction to geophysical prospecting, 4th edition, McGraw-Hill Book Co., 867 P.
6. Egyptian Geological Survey and Mining Authority (EGSMA), (2003): Geological map of the study area.
7. Egyptian Geological Survey and Mining Authority (EGSMA), (2003): Total Magnetic intensity map of Sinai, Egypt, Scale 1: 500,000.
8. Egyptian Geological Survey and Mining Authority (EGSMA), (2003): Bouguer anomaly map of Sinai, Egypt, Scale 1: 500,000.
9. Geosoft (2014): Geosoft Oasis Montaj, Ver. 8.3.3 Software for Earth science, Geo-soft Inc., Toronto, Canada.
10. GM-SYS (2014): GM-SYS®, Gravity and Magnetic Modeling Version 4.9 (Northwest Geophysical Association Inc., Corvallis, Oregon, U.S.A.).
11. Henderson, R. G., and Zietz, I., (1949): The Computation of Second Vertical Derivatives of geomagnetic fields. Geophysics, Vol. 14.
12. Kearey, P. and Brooks, M., (1994): An introduction to geophysical exploration: Blackwell Scientific Publication, London, 254p.
13. Macleod, I. N., Vierra, s., and Chaves, A. C., (1993): Analysis signal and reduction to the pole in the interpretation total magnetic field data at low magnetic latitudes. Proceeding of the third international congress of the Brazilian society of the geophysics.
14. Milsom, J., (1989): Field Geophysics. Milton Keynes: Open University Press.
15. Miller, H. G., and Singh, V., (1994): Potential field tilt A new concept for location of potential field sources: Jour. of applied geophysics, Vol.32, pp.213-217.
16. Moustafa, A. M. (1973): Block faulting in the Gulf of Suez: proceeding of the 5th Egyptian general petroleum corporation Exploration seminar, 35p.
17. Moustafa, A. R. (1993): Structural characteristics and tectonic evolution of the east margin blocks of the Suez rift: Tectonophysics, v. 223, p.381-399.
18. Nettleton, L. L., (1976): Gravity and magnetic in oil prospecting. McGraw-Hill Book Co. Inc., New York, 322 p.
19. Oruc, B., and Keskinezer, A., (2008): Structural setting of the northeastern Biga peninsula (Turkey) from Tilt Derivatives of gravity gradient Tensors and magnitude of horizontal gravity components. Pure and applied geophysics, Vol.165, Issue 9-10, pp.1913-1927.
20. Phillips, J. D., (1998): Processing and interpretation of aeromagnetic data for the Santa Cruz Basin-Patahonia Mountains area, south – central Arizona, U.S. geophysical survey open – file report, pp.02-98.
21. Phillips, J. D., (2000): Locating magnetic contacts: a comparison of the horizontal gradient, analytic signal, and local wavenumber methods: Society of Exploration Geophysicists, Expanded Abstracts, 2000 Technical Program, 1, 402–405. Online.
22. ftp://ftpext.usgs.gov/pub/cr/co/denver/musette/pub/outside_pubs/jeff/Phillips_SEG2000.pdf.
23. Reid, A. B., Allsop, J. M., Granser, H., Millett, A.J., and Somerton, I. W., (1990): Magnetic interpretation in three dimensions using Euler Deconvolution. Geophys., V. 55, pp.80-91.
24. Roest, W. R., Verhoef, J. and Pilkington, M. (1992): Magnetic interpretation using the 3D analytic signal: Geophysics, 57, 116–125.
25. Verduzco, B., Fairhead, J. D., Green, C. M., and Mackenzie, C., (2004): New insights into magnetic derivative for structural mapping. The Leading Edge, Vol. 23, pp. 116-119.
26. Werner, S., (1953): Interpretation of magnetic anomalies at sheet Like bodies: Sveriges Geol. Undersok., Ser. C, Arsbok. 43 (1949), No.6.

9/13/2017